Effect of Coulomb friction on orientational correlation and velocity distribution functions in a sheared dilute granular gas

Bishakhdatta Gayen* and Meheboob Alam†

Engineering Mechanics Unit, Jawaharlal Nehru Centre for Advanced Scientific Research, Jakkur P.O., Bangalore 560064, India

(Received 18 February 2011; revised manuscript received 4 July 2011; published 12 August 2011)

From particle simulations of a sheared frictional granular gas, we show that the Coulomb friction can have dramatic effects on orientational correlation as well as on both the translational and angular velocity distribution functions even in the Boltzmann (dilute) limit. The dependence of orientational correlation on friction coefficient (μ) is found to be *nonmonotonic*, and the Coulomb friction plays a dual role of enhancing or diminishing the orientational correlation, depending on the value of the tangential restitution coefficient (which characterizes the roughness of particles). From the sticking limit (i.e., with no sliding contact) of rough particles, decreasing the Coulomb friction is found to reduce the density and spatial velocity correlations which, together with diminished orientational correlation for small enough μ, are responsible for the transition from non-Gaussian to Gaussian distribution functions in the double limit of small friction ($\mu \to 0$) and nearly elastic particles ($e \to 1$). This double limit in fact corresponds to perfectly smooth particles, and hence the Maxwellian (Gaussian) is indeed a solution of the Boltzmann equation for a frictional granular gas in the limit of elastic collisions and zero Coulomb friction at any roughness. The high-velocity tails of both distribution functions seem to follow stretched exponentials even in the presence of Coulomb friction, and the related velocity exponents deviate strongly from a Gaussian with increasing friction.

DOI: 10.1103/PhysRevE.84.021304 PACS number(s): 45.70.Mg, 47.45.−n

I. INTRODUCTION

Granular gases, a collection of macroscopic particles under external forcing, resemble molecular gases with particle interactions being binary and instantaneous [1]; the dissipative nature of particle collisions requires external pumping of energy into the system so as to maintain the fluidized state of particles. The well-established dense gas kinetic theory has been appropriately modified in formulating the theory of rapid granular gases by incorporating the inelastic nature of particle collisions [2–4]. The concept of coarse-graining over single-particle distribution function is utilized while making a transition from the particle-level properties to the macroscale (hydrodynamic) fields, leading to appropriate balance equations for hydrodynamic fields. It may be noted that the molecular gases possess a thermodynamic equilibrium, with Maxwell-Boltzmann (Maxwellian, Gaussian) distribution playing the role of the equilibrium distribution function. This thermodynamic equilibrium corresponds to a *uniform, homogeneous* state of constant density and temperature with zero macroscopic velocity.

In contrast to molecular gases, the collisional dissipation does not permit granular gases to evolve toward any equilibrium uniform state [1,2]. The simplest "nondriven" granular system is the *homogeneous cooling state* (HCS), which corresponds to a collection of randomly moving particles with some initial granular temperature and *zero* macroscopic velocity. The HCS is a *spatially* homogeneous state since both the number density and the granular temperature remain homogeneous (constant) in space (and the macroscopic velocity is always zero), but the granular temperature decays with time [$T(t) \sim (1 + t/\tau)^{-2}$, where τ is the relaxation time that depends on the restitution coefficient, $e \neq 1$, the number density n, and the initial temperature $T(0)$] due to collisional dissipation. For HCS, the Boltzmann equation can be reduced to a time-independent equation for the "scaled" velocity distribution function [5]—the solution of this scaled equation has been obtained via *perturbation methods*, with its zeroth-order solution being a Maxwellian (Gaussian) that holds for $e \to 1$. The non-Gaussian corrections can be expressed in terms of Sonine polynomials (or any other orthogonal polynomials), and the first nontrivial correction is given in terms of the fourth velocity cumulant, which is proportional to *inelasticity* $\epsilon = (1 - e^2)$ [2,5] and hence vanishes in the elastic limit ($e \to 1$). Therefore the velocity distribution function (VDF) of HCS is non-Gaussian at any finite dissipation ($e \neq 1$). (It may be noted that the radius of convergence of the above mentioned perturbation solution of the inelastic Boltzmann equation is still debated [6].) Apart from undriven HCS of a granular gas, there also exists nonequilibrium steady-states for various "driven" granular flow configurations (e.g., vibrated bed, simple shear flow, etc.) for which the Maxwellian (Gaussian) still remains the leading-order velocity distribution in the double limit of both Knudsen number and inelasticity approaching zero [4].

The non-Gaussian nature of velocity distribution function of granular gases has been studied in a variety of driven and undriven granular gases using theory [4,7,8], simulation [9–17] and experiment [18–24]. As mentioned above [2,4,5], the low-velocity regions of the VDF (i.e., for particle velocities that are equal to or less than the thermal velocity) can be approximated in terms of Sonine polynomials with the Maxwellian being the zeroth-order solution. However, the high-velocity tails of VDFs can differ significantly from a Gaussian, depending on the restitution coefficient, and has been characterized in terms of a stretched exponential [8,19], or an exponential [7,24], or

*Present address: Department of Mechanical and Aerospace Engineering, University of California at San Diego, CA 92093, USA.

†Corresponding author: meheboob@jncasr.ac.in

a power law [17]. The tails of a VDF correspond to particle velocities that are much larger than the thermal velocity. More importantly, it has been recently shown for HCSs [6] that the Sonine expansions are nonconvergent (though asymptotic and Borel resummable) at large inelasticity due to the exponential tails of VDF.

Considering the "large-velocity" asymptotic limit of the Boltzmann equation for HCSs, Esipov and Pöschel [7] showed that the high-velocity tails decay as $f \sim \exp[-\delta v/v_0(t)]$, where $v_0(t) = \sqrt{T(t)}$ is the time dependent thermal velocity and $\delta \sim \epsilon^{-1} = (1-e^2)^{-1}$ is a constant. For both undriven (HCS) and driven homogeneous granular gases, van Noije and Ernst [8] obtained analytical expressions for the single particle velocity distribution function by solving the Enskog-Boltzmann equation perturbatively in terms of Sonine polynomials. They further showed that the high energy tails of velocity distributions in the driven case satisfy a stretched exponential of the $f \sim \exp(-\delta v^\alpha)$, where v is the velocity scaled by the thermal velocity, $\alpha = 1.5$ and $\delta \sim O(\epsilon^{-1})$. These predictions of exponential and stretched exponential VDFs have been verified in various simulations [11–14] as well as in experiments [19,24]. The most recent experiments of Tatsumi *et al.* [24] demonstrated that while the exponent α is close to 1.5 in a steady driven system, its value evolves with time from 1.5 to 1 in a freely cooling system. It is clear that the theory and experiment on VDFs agree with each other for both driven and undriven granular gases of *smooth* particles (for which rotational degrees of freedom do not play any role).

Literature on velocity distribution functions and correlations in *frictional*, *rough* granular gases is very scarce. One reason could be that the Coulomb friction might not be important in a granular gas or it is nontrivial (difficult) to model Coulomb friction in any theory, presumably the latter. However, friction is known to be very important in dense granular materials [25–28]; the effect of Coulomb friction on various properties of dense granular materials, especially on rheology and jamming, are currently being investigated by many researchers [25,29]. The earliest works of Walton and Braun [30,31] and Lun [32] probed the rheology of a rough granular gas (with Coulomb friction) for a range of densities up to the freezing density, and the latter work [32] also validated a related kinetic theory constitutive model [3]. Another related work is that of Jenkins and Zhang [33] who incorporated Coulomb friction in the kinetic theory of dense, collisional flows of slightly frictional particles in the quasielastic limit. *Our focus is, however, in the opposite limit of a dilute granular gas for which the Coulomb friction is found to be equally important as we show in this paper.*

The earliest work on the effect of Coulomb friction on the mean field quantities (translational and rotational granular temperatures) seems to be that of Huthmann and Zippelius [34], and the most comprehensive recent simulation and theoretical work is that Herbst *et al.* [35]. However, none of these papers probed particle-level properties like the velocity distribution functions and correlations. The only work that probed the effect of Coulomb friction on VDFs of a driven granular gas is that Goldhirsch *et al.* [36] who solved Boltzmann equation perturbatively in the limit of smooth particles with small friction for a sheared granular gas. Cafiero *et al.* [37] showed that, under stochastic rotational driving of a granular gas (without Coulomb friction), the translational velocity fluctuations are non-Gaussian but the angular velocity fluctuations remain Gaussian. Recent experiments of Schmick and Markus [22] indeed found Gaussian angular velocity distributions for a wide range of parameters; in these experiments the rotational driving was achieved by an alternating magnetic field interacting with magnetic dipoles embedded in spheres.

This paper is a sequel to our previous paper [38] on the uniform shear flow of a dilute (i.e., the Boltzmann limit) rough granular gas. The adopted collision model had only tangential restitution (β) to model the roughness of particles in an approximate manner. From event driven simulations, it was shown [38] that both the translational and rotational velocity fluctuations remain close to a Gaussian at perfectly smooth and rough limits for elastic collisions ($e = 1$). Away from these two limits, the orientational as well as velocity correlations are responsible for the emergence of non-Gaussian high-velocity tails that follow stretched exponentials. Another important finding of Ref. [38] is that the translational and rotational velocities are strongly coupled (dubbed orientational correlation), however, there is no orientational correlation-induced singularity at perfectly smooth and rough limits for elastic collisions ($e = 1$). The latter observation is in contrast to that in a freely cooling granular gas [39].

The effect of Coulomb friction on velocity distributions and various correlations was neglected in Ref. [38], which is the central focus of this paper. Here we use Walton's collision model [30,31] that incorporates both tangential restitution and Coulomb friction along with normal restitution coefficient as in Sec. II. The justification of this three-parameter collision model and the related literature are given in Sec. II B. The role of Coulomb friction on temperature ratio and particle clustering is discussed in Sec. III A, orientational correlation in Sec. III B, velocity distribution functions in Sec. III C, and density and velocity correlations in Sec. III D. We conclude with a brief discussion of the pertinent Boltzmann equation for a frictional granular gas in Sec. IV.

II. COLLISION MODEL AND SIMULATION METHOD

Our simulations are based on *inelastic* rough hard spheres (of diameter d, mass m, and the moment of inertia I) for which the interaction potential is purely repulsive with dissipative frictional collisions. In the absence of any external force, the particles move in straight lines at a constant speed between collisions and change their velocities immediately when a collision occurs. This means that the collisions are instantaneous and the impulsive force comes in the picture at the moment of their collision at the contact point. The *precollisional* translational and angular velocities of particle i are denoted by $\mathbf{v}_i$ and $\boldsymbol{\omega}_i$, respectively, and the corresponding *postcollisional* velocities are denoted by the primed symbols, $\mathbf{v}_i'$ and $\boldsymbol{\omega}_i'$. The total precollisional relative velocity at contact $\mathbf{g}_{ij}$ between particle i and j is given by

$$\mathbf{g}_{ij} = \mathbf{v}_{ij} - \frac{d}{2}\mathbf{k}\times(\boldsymbol{\omega}_i + \boldsymbol{\omega}_j) \equiv \mathbf{g}_n + \mathbf{g}_t, \tag{1}$$

where

$$\mathbf{g}_n = (\mathbf{g}_{ij}\cdot\mathbf{k})\mathbf{k} \quad \text{and} \quad \mathbf{g}_t = \mathbf{k}\times(\mathbf{g}_{ij}\times\mathbf{k}) \tag{2}$$

are the normal and tangential components of the contact velocity, respectively. Here $\mathbf{v}_{ij} = \mathbf{v}_i - \mathbf{v}_j$ is the translational velocity of particle i relative to j, and $\mathbf{k}_{ij} = (\mathbf{r}_j - \mathbf{r}_i)/|\mathbf{r}_j - \mathbf{r}_i| \equiv \mathbf{k}$ is the unit vector directed from the center of the ith particle to that of jth particle.

A. Constant β model

For the simplest model of rough, inelastic spheres, two material parameters are needed to characterize the collision process [3,32,43,44]: (1) the normal coefficient of restitution, e, and (2) the tangential coefficient of restitution, β. The pre- and postcollisional relative velocities of the contact point are related via the following expressions:

$$\mathbf{g}_n' = -e\mathbf{g}_n, \quad \text{and} \quad \mathbf{g}_t' = -\beta\mathbf{g}_t, \tag{3}$$

with primes denoting postcollisional velocities and bare quantities being their precollisional counterparts. In general, $0 \leqslant e \leqslant 1$ and $-1 \leqslant \beta \leqslant 1$. It may be noted that the collision model for perfectly rough ($\beta = 1$), perfectly elastic ($e = 1$), and rigid elastic molecules was originally proposed by Bryan [40] more than one hundred years back. About 25 later, Pidduck [41] incorporated Bryan's model into the kinetic theory; in particular, he generalized the Chapman-Enskog's method and calculated viscosity of rough spherical molecules [42]. The above inelastic version (3) of Bryan's collision model has been used to model rough granular particles in a variety of contexts: (1) to calculate the transport coefficients of rough granular gases from kinetic theory [2,3,5], (2) to validate the kinetic-theory constitutive relations via particle simulations [32,43], and (3) to understand instabilities in unbounded granular shear flow [44].

In the collision model (3), $\beta = -1$ refers to collisions between perfectly smooth particles, with increasing value of β being an indicator of increasing degrees of particle surface friction. The limit of $\beta = 1$ is referred to perfectly rough particles for which the tangential velocity completely reverses it sign (i.e., complete spin reversal) and partial spin reversal occurs for $0 < \beta < 1$; the value of $\beta = 0$ represents the case for which the particle surface roughness and inelasticity are sufficient to eliminate the postcollisional tangential relative velocities. This will henceforth be called the *constant-β model,* which incorporates surface roughness in a gross manner and neglects Coulomb friction (discussed in the next section).

For collisions of rough particles, both linear and angular momentums are conserved; the momentum transfer occurs along the contact normal as well as along the tangent to the contact point. Therefore the collisional impulse (change of momentum after collision) can be decomposed into normal and tangential components:

$$\mathbf{J} = \mathbf{J}_n + \mathbf{J}_t, \tag{4}$$

where the expressions for $\mathbf{J}_n$ and $\mathbf{J}_t$ follow from the conservations of linear and angular momentum of the colliding particle pair:

$$\mathbf{J}_n = -\frac{(1+e)}{2} m\mathbf{g}_n, \tag{5}$$

$$\mathbf{J}_t = \frac{(1+\beta)}{2}(1+\mathcal{I}^{-1})^{-1} m\mathbf{g}_t. \tag{6}$$

Here $\mathcal{I} = 4I/(md^2)$ is the nondimensional moment of inertia of a particle, with $\mathcal{I} = 2/5$ for solid spheres and $2/3$ for a thin-shell sphere.

B. Coulomb friction: Variable-β model

To study the dynamics of frictional particles, we need a realistic collision model of rough particles that takes into account the effect of Coulomb friction. One widely used model is due to Walton [30,31] who proposed a three-parameter model (discussed below): (1) the coefficient of normal restitution (e), (2) the coefficient of tangential restitution (β) that acts during sticking contacts, and (3) the coefficient of Coulomb friction (μ) that acts during sliding or grazing contacts. Later on, Foerster *et al.* [45] carried out a series of experiments to measure collision properties of spheres involved in binary collisions with spheres or with a flat surface, and they found that Walton's collision model provides an accurate description of collision dynamics of spheres as in their experiments. Since then, several researchers adopted Walton's collision model to probe frictional properties of rough granular materials: for example, the numerical simulations of Luding [46] on vertically vibrated granular materials demonstrated the important role of Coulomb friction on the dynamical behavior of this system. More recently, Herbst *et al.* [35] conducted simulations in a two-dimensional heated frictional granular gas, and developed mean-field-type rate equations for both translational and rotational granular temperatures by considering five different limiting cases of Walton's model. They concluded that the theory based on the full frictional model (i.e., Walton's model) is able to reproduce the simulation results quantitatively for all values of friction coefficient. For related issues on different collision models for granular materials, the readers are referred to a recent book [47].

As mentioned, the Coulomb friction helps to distinguish between the sliding and the sticking contacts: in the former case the Coulomb friction decides the tangential component of impulse and in the latter the tangential restitution decides the tangential impulse. When the tangential impulse is greater or equal to the product of the friction coefficient and the normal impulse, the *sliding contact* occurs and the following equality holds:

$$|\mathbf{J}_t| = \mu|\mathbf{J}_n|. \tag{7}$$

The sliding contact between two spheres leads to dissipation of energy [48]; if this energy loss is large enough to overcome the total relative tangential velocity of colliding spheres, they cease to slide past each other, and hence the contact becomes a sticking one. Therefore, for real particles, all contacts cannot be sliding and we must take account of both sliding and sticking contacts in any realistic contact model of particle collisions.

If the tangential impulse is less than the product of the friction coefficient and the normal impulse, i.e., $|\mathbf{k} \times \mathbf{J}| < \mu|\mathbf{k} \cdot \mathbf{J}|$, the *sticking* contact occurs. The tangential velocity of the contact point is

$$\mathbf{g}_t' = -\beta_0\mathbf{g}_t, \tag{8}$$

where β_0 is a phenomenological constant, characterizing the restitution of velocity in the tangential direction for sticking contacts, with $-1 \leqslant \beta_0 \leqslant 1$. From experiments, it has been

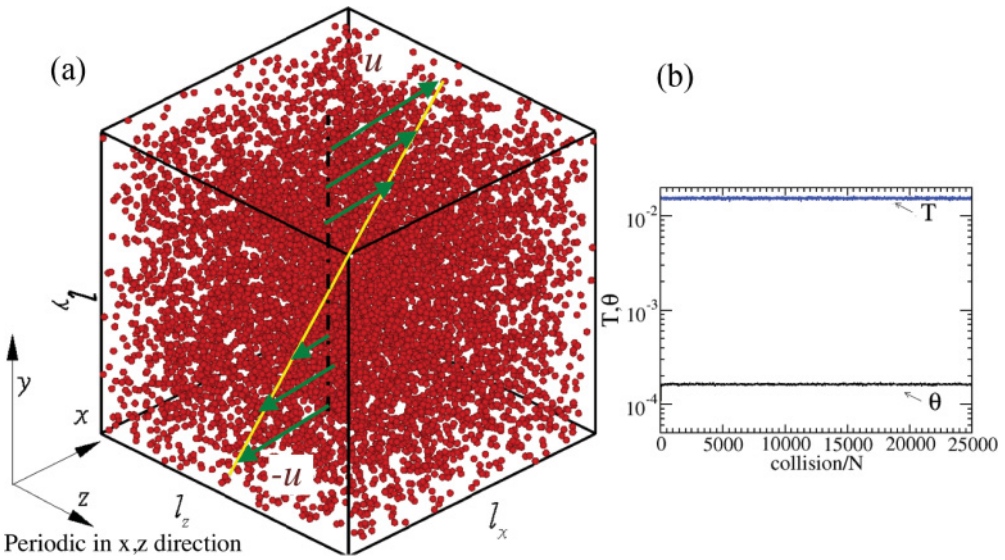

FIG. 1. (Color online) (a) Schematic of granular shear flow with linear velocity profile. (b) Time evolution of translational (T, upper curve) and rotational (θ, lower curve) granular temperatures. Parameter values are $\phi = 0.01$, $N = 8000$, $e = 0.5$, $\beta_0 = 0$, and $\mu = 0.01$.

found that typical values of β_0 and μ are 0.4 and 0.123, respectively, for commercial ball bearings [49,50] and $\beta_0 = 0.44$ and $\mu = 0.09$ for glass beads [45]. A positive value for β_0 in Eq. (8) implies that the relative tangential velocity of colliding particles cannot only go to zero but also reverses its sign—the origin of this sign reversal can be tied to the release of the tangential strain energy in the contact region [49,50]. Therefore the spin reversal [$\beta_0 > 0$, Eq. (8)] indeed occurs for real particles [45,49,50] and is not an artefact of the adopted contact model.

From Eqs. (5)–(7), the tangential coefficient of restitution can be found explicitly as

$$\beta(\Phi) = -1 + \mu(1+e)(1+\mathcal{I}^{-1})\frac{|\mathbf{k}\cdot\mathbf{g}_{ij}|}{|\mathbf{k}\times\mathbf{g}_{ij}|} \equiv -1 + \mu(1+e)(1+\mathcal{I}^{-1})\cot\Phi. \tag{9}$$

Here Φ is the *impact* angle, which is defined as the angle between the contact vector $\mathbf{k}$ and the relative velocity at the contact of two particles:

$$\cos\Phi = \frac{\mathbf{k}\cdot\mathbf{g}_{ij}}{|\mathbf{g}_{ij}|}, \quad \text{with} \quad 0 \leqslant \Phi \leqslant \frac{\pi}{2}. \tag{10}$$

Let us define a critical angle Φ_0 such that when $\Phi > \Phi_0$ there is *sliding* (Coulomb friction) during a collision and when $\Phi \leqslant \Phi_0$ there is *sticking* contact (or the particles are rough). With $\beta = \beta_0$ at $\Phi = \Phi_0$, an expression for this critical angle immediately follows from Eq. (9):

$$\cot\Phi_0 = \frac{\mathcal{I}(1+\beta_0)}{\mu(1+e)(1+\mathcal{I})}. \tag{11}$$

In all simulations the value of β is chosen from $\beta(\Phi)$ and β_0 such that

$$\beta(\Phi) = \min\{\beta_0, -1 + (1+\beta_0)\tan\Phi_0\cot\Phi\}. \tag{12}$$

Note that this model distinguishes between sliding and sticking contacts: there is a sliding contact for $-1 \leqslant \beta(\Phi) < \beta_0$ and a sticking contact for $\beta(\Phi) \geqslant \beta_0$. The collision model with impact-angle-dependent tangential restitution coefficient (12),

$$\mathbf{g}_n' = -e\mathbf{g}_n, \quad \text{and} \quad \mathbf{g}_t' = -\beta(\Phi)\mathbf{g}_t, \tag{13}$$

will henceforth be referred to as the *variable-β model*.

It is clear that the constant-β model can be obtained from the variable-β model in the limit of infinite friction. This holds since the sliding contacts are inhibited in the limit $\mu \to \infty$ and hence the collisions are always sticking with constant tangential restitution coefficient as modeled by Eq. (3).

C. Simulation method

Both the constant-β and variable-β collision models are implemented in an event-driven code [47,51] to simulate the dynamics of frictional spheres under uniform shear. The particles (spheres) are randomly placed in a cubic box with random initial velocity, which is taken from a Gaussian distribution. To achieve the state of *uniform shear flow*, we have used the well-known Lees-Edward boundary condition [52] along the gradient direction (y), with periodic boundary conditions along streamwise (x) and spanwise (z) directions as depicted in Fig. 1(a). To reduce the computational time for a large number of particles, the search algorithm of Lubachevsky [53] has been implemented as in our previous work [38]. In a shear flow the work is done on the system due to the imposed shear field, and there is dissipation of granular energy due to particle collisions. The balance between the shear work and collisional dissipation results in a *nonequilibrium steady state* of uniform shear with constant granular temperature and number density [44]. Figure 1(b) shows the time evolution of translational (T) and rotational (θ) granular temperatures:

$$T = \frac{1}{3}\langle\mathbf{C}\cdot\mathbf{C}\rangle, \tag{14a}$$

$$\theta = \frac{I}{3m}\langle\boldsymbol{\Omega}\cdot\boldsymbol{\Omega}\rangle, \tag{14b}$$

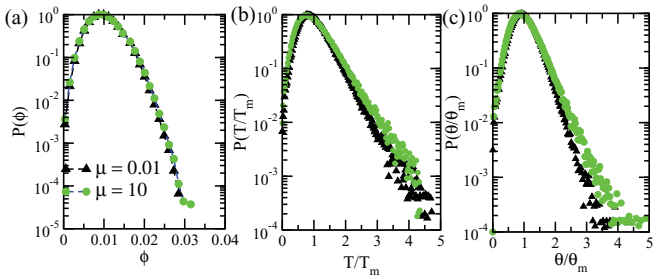

FIG. 2. (Color online) Probability distributions of (a) mean density, (b) translational, and (c) rotational granular temperatures, respectively, for $\phi = 0.01$, $N = 8000$, $\beta_0 = 0$, and $e = 0.5$ for different values of μ.

where $\mathbf{C} = \mathbf{v} - \langle \mathbf{v} \rangle$ and $\Omega = \boldsymbol{\omega} - \langle \boldsymbol{\omega} \rangle$ are the fluctuating (peculiar) translational and rotational velocities, respectively. [Clearly, by definition, the granular temperature is a measure of the kinetic energy associated with particles' fluctuation motion (with the mean motion being subtracted out) and hence dubbed "fluctuation" kinetic energy of particles.] It is clear from Fig. 1(b) that both temperatures reach well-defined statistical mean values after a short transient period. Other macroscopic properties of the flow also remain invariant in time once the system has reached a statistical steady state at which the measurements of various quantities are carried out. Typically, we have discarded data for first 8000 collisions per particle and the simulation was continued until 25 000 collisions per particle.

In the next section (Sec. III), we present simulation results with the Coulomb friction model as discussed in Sec. II B and contrast them with those for the constant-β model as discussed in Sec. II A. Recall that in contrast to the constant-β model, the impact-angle dependent tangential restitution coefficient $\beta(\Phi)$, Eq. (12), is used to identify the sliding or sticking type of collisions in the variable-β model. The effects of Coulomb friction on the temperature ratio θ/T, orientation correlation, velocity distribution functions, and density and spatial velocity correlations are systematically unveiled in Secs. III A–III D.

III. RESULTS: CRUCIAL ROLE OF COULOMB FRICTION AND ROUGHNESS

We present results for a particle volume fraction of $\phi = 0.01$ that corresponds to the Boltzmann limit ($\phi \to 0$) of a dilute granular gas, with the number of particles being $N = 8000$. It may be noted that the results were checked by using $N = 4000$ and 16 000, with no discernible difference as in our previous study [38] (without Coulomb friction).

A. Possible clustering and temperature ratio

Since particle clustering or density inhomogeneity (inhomogeneous distribution of particles) is known to affect the microscopic and rheological properties of a granular gas [54], we first need to ascertain whether the particles are homogeneously distributed or not in the computational box. To this end, we probe the distribution of mean density (ϕ, volume fraction of particles) by dividing the computational box into $8 \times 8 \times 8$ cells such that there are about 15 particles in each cell. In Fig. 2(a), the normalized probability distribution of

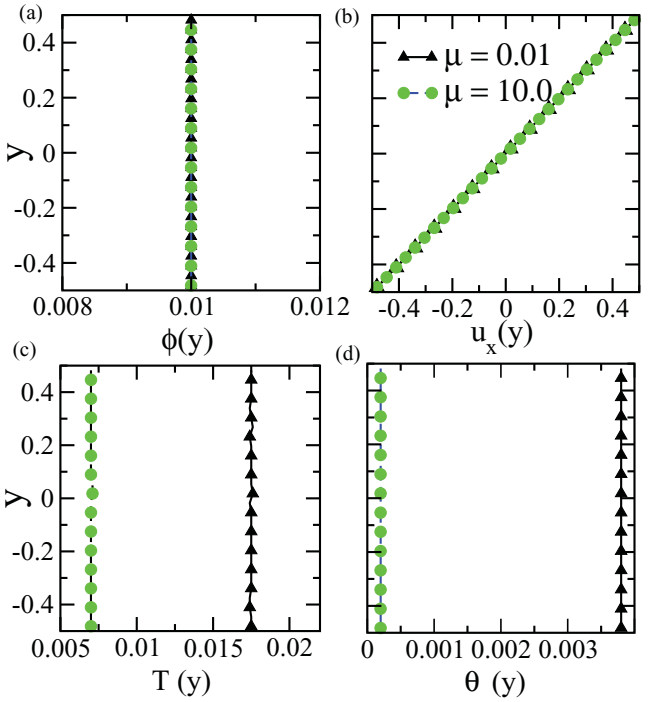

FIG. 3. (Color online) Profiles of (a) density (ϕ), (b) streamwise velocity (u_x), (c) translational granular temperature (T), and (d) rotational granular temperature (θ), respectively. Parameter values are $\phi = 0.01$, $N = 8000$, $\beta_0 = 0$, and $e = 0.5$.

density is shown for two values of friction coefficient for a very dissipative gas ($e = 0.5$). It is observed that there is no friction-induced density inhomogeneity in the system even at $e = 0.5$; for all dissipation levels the local density varies from 0.004 to 0.017 in about 90% cells. In Figs. 2(b) and 2(c), the normalized probability distributions of translational and rotational temperatures are shown, respectively; these distributions also remain relatively unchanged (except the tail regions) with increasing friction. The variance of each distribution remains relatively unaffected by the Coulomb friction.

Although there is a slight variation of mean density and temperatures in different regions of the computational box (Fig. 2), we have found that the density and the translational and rotational temperatures remain constant across the gradient (y) direction as shown in Fig. 3. All these bin-averaged quantities are calculated by dividing the computational box into 15 bins along the y direction [see Fig. 1(a)], and then taking averages over a few thousand collisions per particle. It is also clear from Fig. 3(b) that the streamwise component of the mean velocity u_x is linearly varying along the gradient direction (the other two velocity components, u_y and u_z, remain zero) and hence the system is under uniform shear. Note in Fig. 3 that the Coulomb friction ($\mu = 0.01$, 10) does not change the above observations.

For the constant-β model, the variation of the temperature ratio, $\theta/(\theta + T)$, with the tangential restitution coefficient β is shown in Fig. 4(a) for three values of normal restitution coefficient (e). The black dashed line represents the theoretical

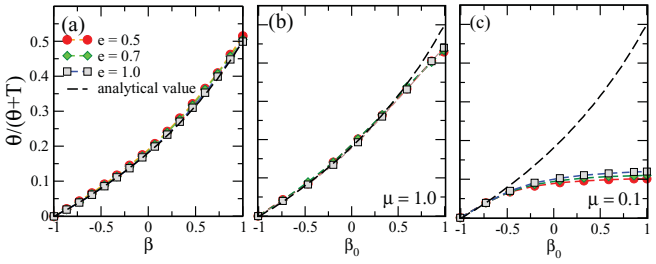

FIG. 4. (Color online) (a) Effect of roughness on temperature ratio $\theta/(\theta+T)$ for different values of e for $\phi = 0.01$ with constant-β model. Temperature ratio based on variable-β model for (b) $\mu = 0.1$ and (c) $\mu = 1$, with $\beta_0 = 0$.

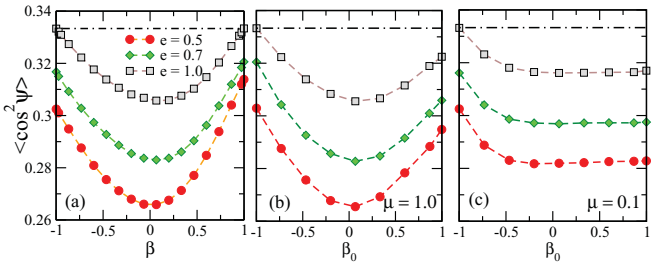

FIG. 5. (Color online) (a) Effect of roughness on orientational correlation for different values of e for $\phi = 0.01$ for constant-β model. Variable-β model: (b) $\mu = 1$ and (c) $\mu = 0.1$ The dot-dashed line in each plot corresponds to $\Lambda = 1/3$.

prediction for temperature ratio [44] using a Navier-Stokes order constitutive model of rough particles [3]:

$$\frac{\theta}{\theta+T} = \frac{\eta_2}{1+\eta_2(1-\mathcal{I}^{-1})}, \tag{15}$$

where $\eta_2 = (1+\beta)/2(1+\mathcal{I}^{-1})$. The translational and rotational energies are equally partitioned [$\theta = T$, i.e., $\theta/(\theta+T) = 1/2$] for only perfectly rough particles ($\beta = 1$) with $e = 1$. The nonequipartition of energy prevails at other values of β; even for $\beta = 1$, $\theta \neq T$ at $e < 1$. The simulation data in Fig. 4(a) suggest that there is a weak dependence of the temperature ratio on e but the theoretical prediction of Eq. (15) is independent of e. It is interesting to note that a Navier-Stokes-level constitutive model [3] gives good prediction for the temperature ratio for the whole range of β at $e = 1$.

Moving to the variable-β model, the effect of critical roughness parameter β_0 on the temperature ratio is plotted for different values of e, setting the Coulomb friction to $\mu = 1$ and 0.1 in Figs. 4(b) and 4(c), respectively. For large friction ($\mu = 10$, not shown), the results resemble those for the constant-β model as in Fig. 4(a). The temperature ratio is seen to be independent of the normal restitution coefficient at $\mu = 1$ as in Fig. 4(b); note that the equipartition of energy does not hold even for $\beta = 1$ with $e = 1$—this is due to additional energy loss due to Coulomb friction. At lower values of Coulomb friction ($\mu = 0.1$), the temperature ratio monotonically increases from the smooth limit ($\beta_0 = -1$) and becomes independent of β_0 for $\beta_0 > 0$, and hence deviates from the the constant-β model for $0 < \beta_0 < 1$. This deviation increases if we increase collisional dissipation.

B. Orientational correlation: Coupling between translation and rotation

It has been recently reported that the translational and rotational fluctuating velocities are strongly correlated in direction in both undriven (freely cooling [39]) and driven (sheared [38]) granular gases, even though they are uncorrelated in a molecular gas—this is an additional property of a frictional granular gas, and adds to one of the many differences between molecular and granular gases. The coupling between orientational and translational velocities has been dubbed "orientational correlation" [38,39]. This correlation can be quantified [38,39] in terms of the peculiar translational and rotational velocities:

$$\Lambda(t) = \frac{1}{N}\sum_{i=1}^{N}\frac{(\mathbf{C}_i\cdot\boldsymbol{\Omega}_i)^2}{(C_i^2\Omega_i^2)} = \frac{1}{N}\sum_{i=1}^{N}\cos^2\Psi_i \equiv \cos^2\boldsymbol{\Psi}, \tag{16}$$

where $\boldsymbol{\Psi}$ is the angle between $\mathbf{C} = \mathbf{v} - \langle\mathbf{v}\rangle$ and $\boldsymbol{\Omega} = \boldsymbol{\omega} - \langle\boldsymbol{\omega}\rangle$. In other words, the mean square of the cosine of the angle between $\mathbf{C}$ and $\boldsymbol{\Omega}$ is a measure of orientational correlation; for a molecular gas, $\Lambda = 1/3$.

First we consider results for the constant-β model for which $\mu \to \infty$: Fig. 5(a) shows the effect of particle roughness (β) on $\langle\Lambda(t)\rangle$ for three values of normal restitution coefficient (e). The dot-dashed line represents the limiting value of $\langle\Lambda(t)\rangle = 1/3$ for a molecular gas; it is seen that $\langle\Lambda(t)\rangle$ deviates from $1/3$ for all e, signaling the presence of orientational correlation. For any value of e, the orientational correlation is maximum at $\beta \sim 0$ and it decreases monotonically as we approach the perfectly smooth ($\beta = -1$) and perfectly rough ($\beta = 1$) limits. As discussed previously [38], this latter observation is in contrast to that in a freely cooling granular gas [39] for which $\langle\Lambda(t)\rangle$ varies nonmonotonically with β for $-1 < \beta < 0$ and $0 < \beta < 1$. Another important observation is that the case of quasielastic collisions ($e \sim 1$) appears to be nonsingular in a sheared granular gas in the sense that the orientational correlation smoothly decreases to its uncorrelated value ($1/3$) for both the perfectly smooth ($\beta = -1$) and rough ($\beta = 1$) limits.

The friction coefficient μ has a pronounced effect on orientational correlation as depicted in Fig. 5(b) ($\mu = 1$) and 5(c) ($\mu = 0.1$). For a given μ, $\langle\Lambda(t)\rangle$ is calculated by varying the critical roughness β_0 following Eqs. (11) and (12). For larger friction [$\mu = 1$, Fig. 5(b)], the orientational correlation follows the same trend with roughness as in the case of constant-β model [Fig. 5(a)]; however, $\langle\Lambda(t)\rangle$ deviates from $1/3$ at the perfectly rough limit ($\beta_0 = 1$) even for the elastic case ($e = 1$). For small values of friction [$\mu = 0.1$, Fig. 5(c)], $\langle\Lambda(t)\rangle$ decreases with increasing roughness (β) from the smooth particle limit ($\beta = -1$) and becomes independent of the critical roughness parameter, irrespective of normal restitution (e), after a certain value of $\beta_0 \sim -0.75$. Therefore the inclusion of any finite Coulomb friction induces orientational correlation at $\beta_0 = 1$.

A close comparison among three cases ($\mu = \infty$, 1, and 0.1) in Fig. 5 suggests that the Coulomb friction has a *dual role* of enhancing and diminishing the orientational

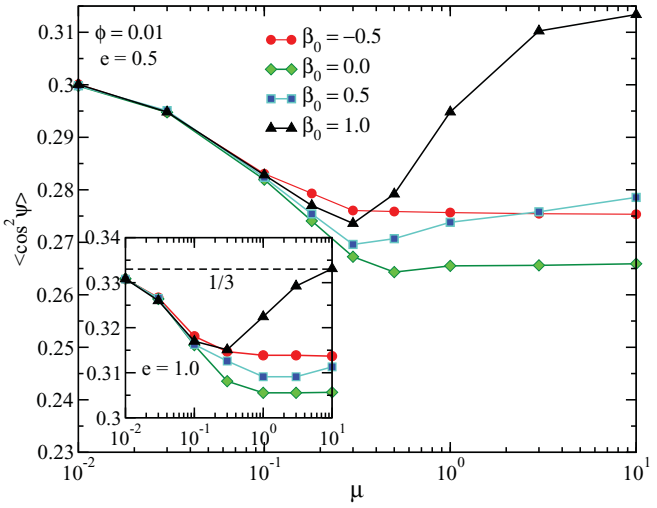

FIG. 6. (Color online) Variation of orientational correlation with friction coefficient (μ) for different values of β_0. Main panel: $e = 0.5$ and inset: $e = 1$; other parameters as in Fig. 5.

correlation, depending on the value of particle roughness (β_0). This is evident from Fig. 6 which shows the variation of $\langle\Lambda(t)\rangle$ with friction coefficient μ for four values of β_0; the trends are similar for both dissipative ($e = 0.5$, main panel) and elastic ($e = 1$, inset) collisions. Near the smooth limit ($\beta_0 = -0.5$, red circles), $\langle\Lambda(t)\rangle$ decreases monotonically with increasing μ; however, this variation becomes nonmonotonic for $\beta_0 > 0$, with the minima of $\langle\Lambda(t)\rangle$ [i.e., the correlation, $= |\langle\Lambda(t)\rangle - 1/3|$, is maximum] occurring at some intermediate values of μ.

It is clear from Fig. 6 that all curves $\langle\Lambda(t)\rangle$ for different values of β_0 coincide with each other if the friction coefficient μ is sufficiently small. This implies that there is a critical value for $\mu = \mu^c$ ($\sim$0.2, which has a weak dependence on β_0) below which ($\mu < \mu^c$) the magnitude of correlation [$= |\langle\Lambda(t)\rangle - 1/3|$] decreases for all β_0, eventually approaching the value for the degenerate case of smooth particles ($\beta = -1$) in the limit of zero friction ($\mu \to 0$). There is also a critical value for $\beta_0 = \beta^c \sim 0$ such that this correlation either decreases with increasing $\mu > \mu^c$ (over $\beta^c < \beta_0 < 1$) or remains constant with increasing $\mu > \mu^c$ (over $-1 < \beta_0 < \beta^c$).

C. Translational and angular velocity distribution functions

The probability distributions of fluctuating/peculiar velocities, $\mathbf{C} = \mathbf{v} - \langle\mathbf{v}^k\rangle$ and $\boldsymbol{\Omega} = \boldsymbol{\omega} - \langle\boldsymbol{\omega}^k\rangle$, are calculated based on cellwise averaging, where $\langle\mathbf{v}^k\rangle$ and $\langle\boldsymbol{\omega}^k\rangle$ denote the mean translational and rotational velocity of the kth cell, respectively. More specifically, the computational box is divided into a number of cells and the cell-averaged velocities (of kth cell) are calculated as follows:

$$\langle\mathbf{v}^k\rangle = \frac{1}{N_k}\sum_j \mathbf{v}_j, \tag{17a}$$

$$\langle\boldsymbol{\omega}^k\rangle = \frac{1}{N_k}\sum_j \boldsymbol{\omega}_j, \tag{17b}$$

with N_k being the number of particles in the kth cell.

It is known from previous theoretical and simulation works [4,55,56] on the uniform shear flow of a smooth granular gas that the VDFs deviate from a Gaussian. Even an approximate Bhatnagar-Gross-Krook (BGK)-type kinetic model [57] can provide an accurate description of the VDFs for small velocities but there are significant discrepancies between theory and simulation at large velocities. It is important to characterize the high-velocity tails of VDFs since it has recently been found [6] that the non-Gaussian (exponential) tails of HCSs are responsible for the nonconvergent behavior (at large inelasticity) of the Sonine expansions for velocity distribution functions. Therefore our primary focus is on the high-velocity tails of VDFs for a frictional granular gas, which seem to follow stretched exponentials in the present flow. In the following, the results are shown only for C_x (the streamwise component of peculiar translational velocity) and Ω_z (the spanwise component of peculiar angular velocity), and other velocity components follow similar behavior (except at low velocities where there are some deviations among VDFs of different velocity components when the dissipation is large enough).

1. *Constant-β model: μ = ∞*

Before presenting results for Coulomb friction, let us discuss a representative set of velocity distribution functions (VDFs) for the constant-β model ($\mu = \infty$) in Fig. 7. The main panels of Figs. 7(a) and 7(b) display the VDFs of C_x and Ω_z, respectively; note that the horizontal axis of each VDF is scaled by the standard deviation of respective VDFs ($\sigma \equiv \sigma_{C_x}$ or σ_{Ω_z}). In each plot, two data sets for $e = 0.5$ (circles) and 1 (squares) have been superimposed and the tangential restitution coefficient has been set to $\beta = 0$; the black dashed line represents a Gaussian distribution. The high-velocity tails ($C_x/\sigma_{C_x}, \Omega_z/\sigma_{\Omega_z} > 3$) of both VDFs are seen to deviate noticeably from a Gaussian even at $e = 1$, and this deviation increases with increasing dissipation ($e = 0.5$).

Focusing on the low-velocity regions of VDFs, we show the variations of the normalized deviation from a Gaussian,

$$D(x) = \left(\frac{P(x)}{\phi(x)} - 1\right), \quad \text{with} \quad x = C_x/\sigma_{C_x}, \Omega_z/\sigma_{\Omega_z}, \tag{18}$$

where $\phi(x) = (2\pi)^{-1/2}\exp(-x^2/2)$ represents a Gaussian, in the upper right insets of Figs. 7(a) and 7(b) for translational and rotational velocities, respectively. It is seen that there are significant deviations from a Gaussian at low velocities ($C_x/\sigma_{C_x}, \Omega_z/\sigma_{\Omega_z} < 2$) even for elastic collisions ($e = 1$). There are two reasons for the observed departure from a Gaussian: (1) the additional dissipation due to tangential restitution ($\beta = 0 \neq -1$) and (2) the imposed shear field ($\nabla\mathbf{u} \neq 0$). These deviations become stronger with decreasing normal restitution coefficient ($e = 0.5$, red circles in upper right insets) for a given roughness β.

Figures 8(a) and 8(b) display the normalized deviation of the VDF of each velocity component, Eq. (18), of translational and rotational velocities, respectively. The deviations of VDFs for different velocity components are almost indistinguishable at $e = 1$ (main panel), but noticeable differences among different velocity components appear at $e = 0.5$ (inset). For

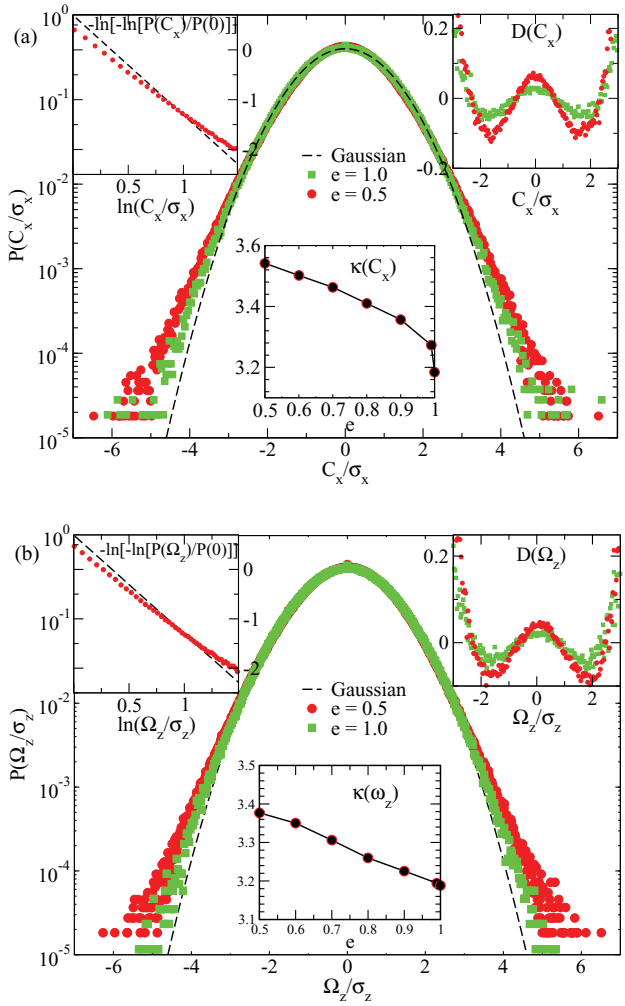

FIG. 7. (Color online) Velocity distribution functions (VDFs) of (a) C_x (main panel) and (b) Ω_z (main panel) for the constant-β model with $\beta = 0$ and $\phi = 0.01$. Top left inset shows the variation of $-\ln\{-\ln[P(x/\sigma)/P(0)]\}$ with $\ln(x/\sigma)$; top right inset depicts the normalized deviation of the respective VDF from a Gaussian, $D(x)$ as defined in Eq. (18), for low velocities; the bottom inset shows the effect of normal restitution coefficient, e, on the kurtosis of each distribution.

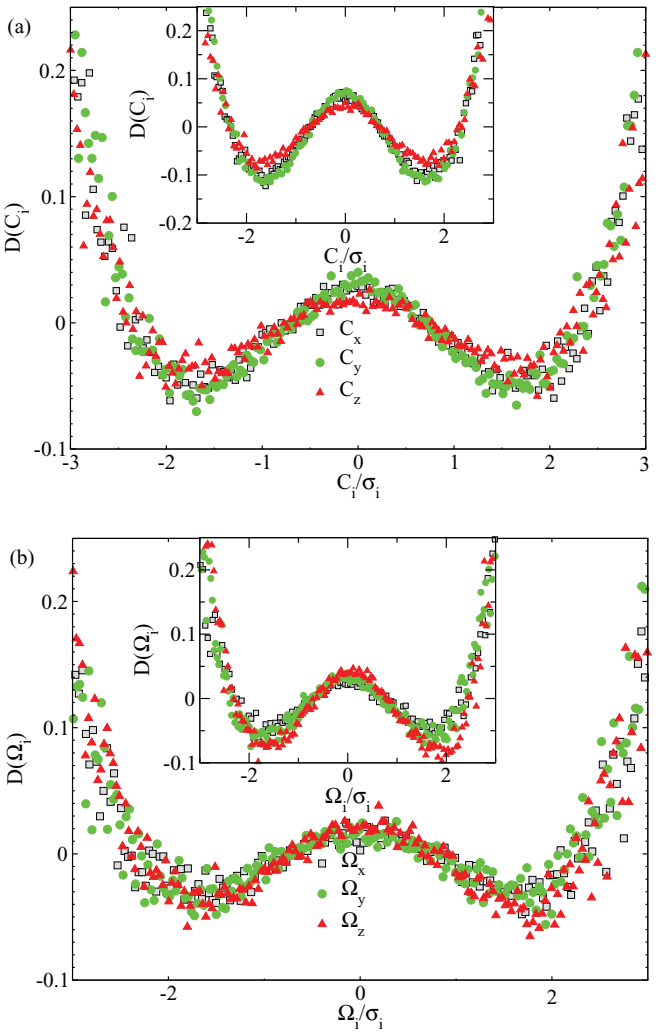

FIG. 8. (Color online) Normalized deviation of VDFs for different velocity components at low velocities: (a) $D(C_i)$ and (b) $D(\Omega_i)$. Main panel: $e = 1.0$; inset: $e = 0.5$; other parameters are as in Fig. 7.

the translational velocity [inset of Fig. 8(a)], the deviations are found to be the least for the z component of velocity (C_z, orthogonal to the shear plane); the VDFs of the velocity components in the shear plane (C_x and C_y) seem to have deviations of same magnitude. For the rotational velocity [inset of Fig. 8(b)], however, the deviation is the largest for Ω_z and the least in the shear plane (Ω_x and Ω_y). This overall trend persists at other parameter values. For all cases, we found that the functional form of the deviations of VDFs from a Gaussian is well represented by a double-well potential in the low-velocity regions. For a smooth granular gas, such deviations have been quantified in terms of the second Sonine polynomial in theory [5,8,11] and experiment [21,23].

In order to quantify the deviation of each VDF from a Gaussian, we have calculated the kurtosis of the distribution:

$$\kappa = \frac{\mu_4}{\mu_2^2}, \tag{19}$$

where

$$\mu_n = \int_{-\infty}^{\infty} (x - \overline{x})^n P(x) dx \tag{20}$$

is the nth moment about the mean of the distribution. The dependence of the kurtosis of $P(C_x)$ and $P(\Omega_z)$ on normal restitution coefficient (e) is shown in the lower insets of Figs. 7(a) and 7(b). For both $P(C_x)$ and $P(\Omega_z)$, $\kappa > 3$, clearly signaling that the VDFs are indeed non-Gaussian for any e at $\beta = 0$.

In our previous work [38] with constant-β model, we have found that the high-velocity tails of the VDFs, such as those in Fig. 7, approximately follow stretched exponentials:

$$P(x) \sim \exp(-\delta x^{\alpha}), \quad \text{with} \quad x = C_x/\sigma_{C_x}, \Omega_z/\sigma_{\Omega_z}, \tag{21}$$

where δ and α are the prefactor and exponent of the distribution, respectively; for a Gaussian distribution, $\delta = 1/2$ and $\alpha = 2$. This implies that in a plot of $-\ln\{-\ln[P(C_x/\sigma_{C_x})/P(0)]\}$ versus $\ln(C_x/\sigma_{C_x})$, the tails would follow a straight line with a slope of α. Such plots are displayed in the upper left insets of Figs. 7(a) and 7(b). To calculate α_{C_x} and α_{Ω_z} from such

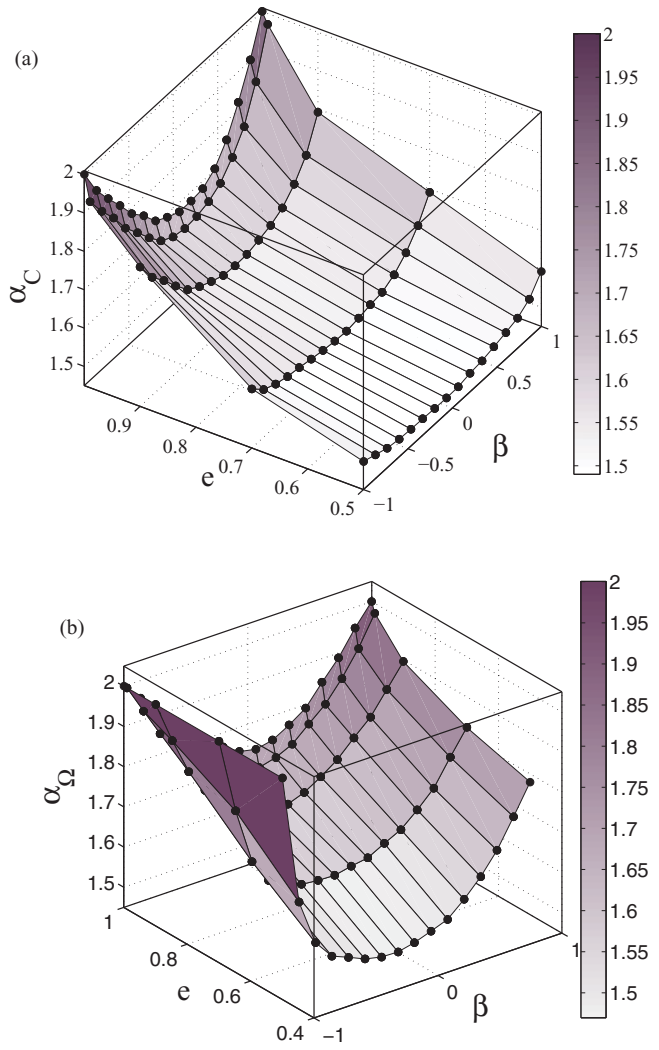

FIG. 9. (Color online) Surface plots for the exponents of tails of (a) $P(C_x)$ and (b) $P(\Omega_z)$ as functions of β and e for constant-β model. Parameter values are as in Fig. 7.

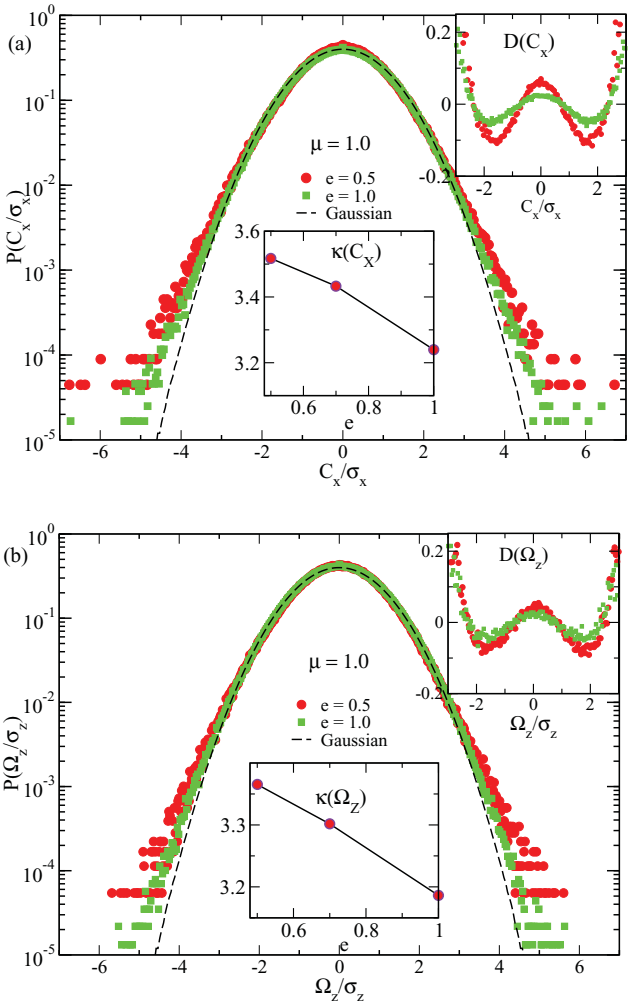

FIG. 10. (Color online) Same as Fig. 7, but for the variable-β model with $\beta_0 = 0$ and $\mu = 1$.

plots, we fit straight line (via the least-square method) to all high-velocity data points that correspond to $\ln(C_x/\sigma_{C_x}) \geqslant 1$ for all velocity components.

The variations of the exponents for the tails of translational (α_{C_x}) and rotational (α_{Ω_z}) velocities as functions of e and β are shown as surface plots in Figs. 9(a) and 9(b), respectively. It is clear that even for perfectly elastic collisions ($e = 1$) the tails of both translational and rotational VDFs deviate from a Gaussian (except at $\beta = \pm 1$ for which $\alpha_C = 2 = \alpha_\Omega$); this deviation is maximum at $\beta \sim 0$. Note that the functional forms of α_{C_x} and α_{Ω_z} are asymmetric and symmetric (around $\beta = 0$), respectively, at $e = 1$. With increasing inelasticity (i.e., decreasing e), both α_{C_x} and α_{Ω_z} decrease sharply, and α_{Ω_z} also becomes asymmetric around $\beta = 0$.

2. *Effect of Coulomb friction on VDFs*

To ascertain the effect of finite Coulomb friction on VDFs, we set the critical roughness to $\beta_0 = 0$ (the results at other values of β_0 are qualitatively similar) and four different values of friction coefficient ($\mu = 10$, 1, 0.1, and 0.01) are investigated using the variable-β model [see Eqs. (11) and (12)]. Typical results are displayed in Figs. 10 and 11 for two values of friction coefficient $\mu = 1$ and 0.01, respectively. [The VDFs of C_x and Ω_z for large friction ($\mu = 10$, not shown) closely resemble those in Fig. 7 for the constant-β model; this is expected since the latter model corresponds to $\mu = \infty$.] For each case, the variation of $-\ln\{-\ln[P(x)/P(0)]\}$ with $\ln(x)$, where $x = C_x/\sigma_{C_x}, \Omega_z/\sigma_{\Omega_z}$, looks similar to those for the constant-β model (the left inset of Fig. 7) and hence is not shown. The top right insets of Fig. 10 display the normalized deviation [Eq. (18)] of VDF at low velocities from a Gaussian, and the bottom insets of Fig. 10 and Fig. 11 show the variations of kurtosis with normal restitution coefficient. When we decrease the value of friction coefficient from $\mu = \infty$ (Fig. 7) to $\mu = 1$ (Fig. 10), the kurtosis of each VDF (lower insets) decreases toward 3, signaling a relatively lesser deviation from a Gaussian. The deviations in the low-velocity regions also decrease with decreasing friction coefficient (compare top right insets of Figs. 7 and 10); note that the functional form of $D(x)$ [Eq. (18)] still retains a double-well potential shape in the presence of Coulomb friction. For very small values of $\mu = 0.01$ (Fig. 11), the kurtosis of each VDF approaches 3 and the respective tails also have exponents $\alpha_i \sim 2$, characterizing

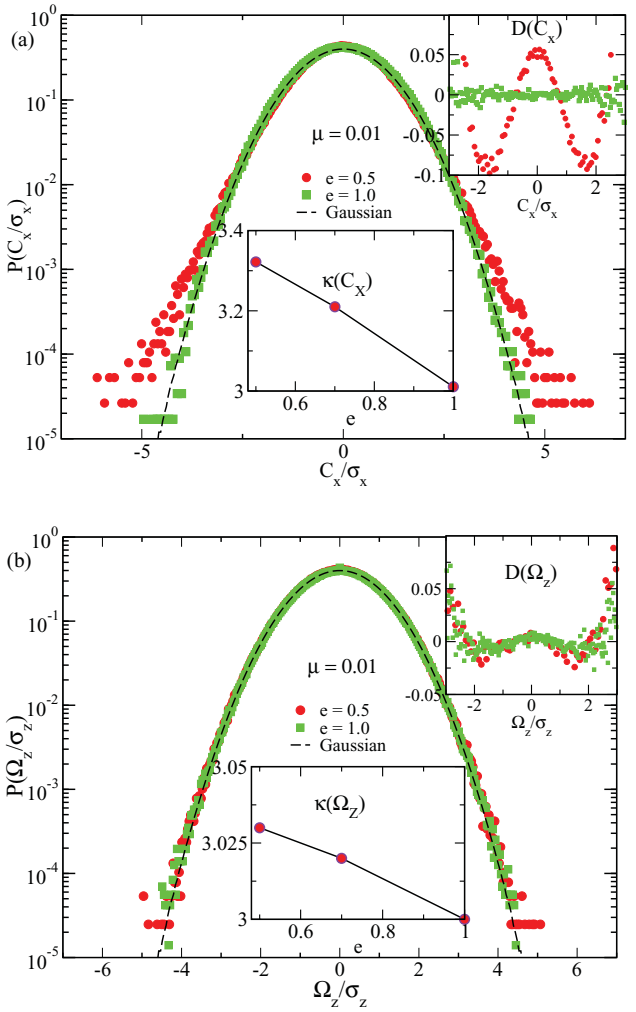

FIG. 11. (Color online) Same as Fig. 10, but for $\mu = 0.01$.

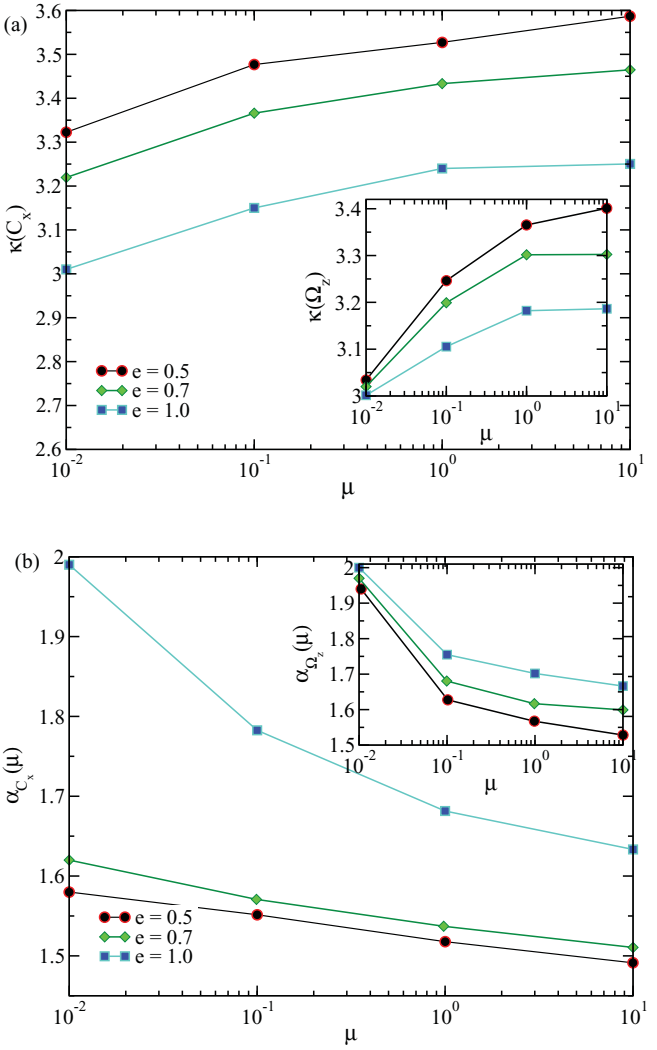

FIG. 12. (Color online) (a) Variations of the kurtosis for streamwise translational and spanwise rotational velocities on friction coefficient μ for different values of e in the main panel and in the inset, respectively. (b) Effect of μ on the exponent of $P(C_x)$ and $P(\Omega_z)$ in the main panel and inset, respectively. Parameter values are $\phi = 0.01$ and $\beta_0 = 0$.

a near Gaussian, for $e = 1$. Of course, even for the latter case of elastic collisions, there are small but finite deviations from a Gaussian due to the nonzero shear field.

The effect of Coulomb friction on the non-Gaussianity of VDFs is summarized in Figs. 12(a) and 12(b). The main panel of Fig. 12(a) shows the variation of the kurtosis of $P(C_x)$ with the friction coefficient (μ) for three different normal restitution coefficients (e), and the inset shows the same for $P(\Omega_z)$; the critical roughness is set to $\beta_0 = 0$. For $e = 1$, the kurtosis of both distributions is close to that of a Gaussian ($\kappa = 3$) for small friction ($\mu = 0.01$), increases with increasing Coulomb friction, and appears to saturate at large enough μ (which corresponds to the limit of constant-β model). With decreasing e, the kurtosis of both distributions strongly deviates from a Gaussian at any μ. The main panel and the inset of Fig. 12(b) show the variations of the exponents of tails of $P(C_x)$ and $P(\Omega_z)$, respectively, with μ for different e. These results mirror those for the kurtosis: the exponents (α_{C_x} and α_{Ω_z}) decrease from the Gaussian limit ($\alpha = 2$) with increasing μ and decreasing e, signaling larger deviations from a Gaussian.

D. Density and velocity correlations

Last, we would like to ascertain the possible role of Coulomb friction as well as that of normal and tangential restitution coefficients on the pair correlation and the spatial velocity correlation functions since both are known to be progenitors of non-Gaussianity of velocity distribution functions in smooth ($\beta = -1$) granular gases [14,17,58,59]. The pair correlation function ($g(r)$) is defined as the probability of finding another particle at a distance r from the test particle; thus $g(r)$ gives information about the local spatial ordering of particles and hence of density correlation. This is calculated from [51]:

$$g(r) = \frac{2V}{N^2}\left\langle \sum_{i-1}^{N}\sum_{j>1}^{N}\delta(r - r_{ij})\right\rangle, \tag{22}$$

where V is the volume and N is the number of particles. Similar information about the spatial correlation between any two components of fluctuating particle velocities is quantified

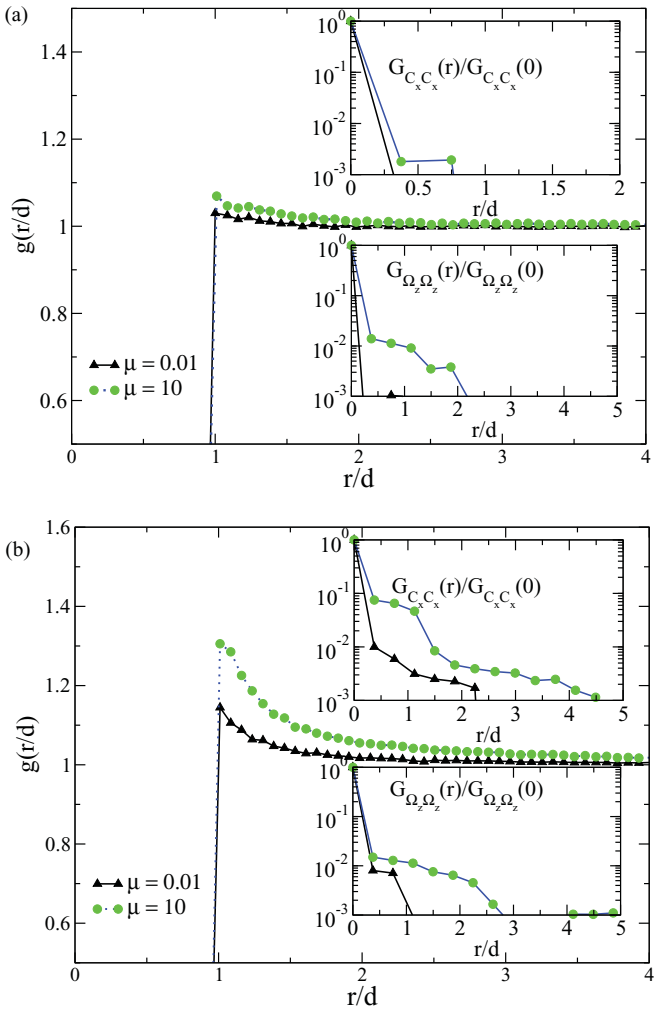

FIG. 13. (Color online) Effect of Coulomb friction on the pair correlation function (main panel), translational velocity correlation (upper inset), and rotational velocity correlation (lower inset) for (a) $e = 1.0$ and (b) $e = 0.5$, with $\phi = 0.01$ and $\beta_0 = 0$.

in terms of the spatial velocity correlation function [51] which is defined as

$$G_{\zeta_i\zeta_j}(r) = \langle \zeta_i(R)\zeta_j(R+r)\rangle, \tag{23}$$

where $i/j = x,y,z$ and $\zeta = C,\Omega$. When particle velocities are random, the correlation is zero; a nonzero value of $G_{\zeta_i\zeta_i}$ indicates correlation.

The effect of Coulomb friction on the pair correlation function of a dilute granular gas ($\phi = 0.01$) can be ascertained from the main panel of Fig. 13(a), which displays the variation of $g(r)$ for two values of friction coefficient $\mu = 10$ (circles) and 0.01 (triangles) at a normal restitution coefficient of $e = 1$. The same set of data at $e = 0.5$ is displayed in Fig. 13(b). For both cases, $g(r)$ remains featureless (i.e., there are no peaks, which implies that there is no "local" spatial ordering of particles) and it behaves almost like a molecular gas. However, the contact value of $g(r/d = 1)$ increases sharply with increasing friction; for a given μ, $g(r/d = 1)$ increases with decreasing e.

The upper and lower insets in Figs. 13(a) and 13(b) display spatial velocity correlations for $\langle C_xC_x\rangle$ and $\langle \Omega_z\Omega_z\rangle$, respectively. (The velocity correlation data for other velocity components, $\langle C_iC_j\rangle$, etc., look similar and hence are not shown.) The velocity correlation increases with increasing μ, and becomes more pronounced at higher dissipations ($e = 0.5$). At $e = 0.5$ and $\mu = 10$ there is a significant correlation of streamwise velocity, $G_{C_xC_x}$, as seen in the top inset of Fig. 13(b); the corresponding correlation for $G_{\Omega_z\Omega_z}$ is relatively weaker than $G_{C_xC_x}$. For given e and roughness β_0, the lower the value of μ the weaker the (both density and velocity) correlations. Collectively, the results in Fig. 13 suggest that the dissipation associated with both Coulomb friction and inelasticity is responsible for enhanced density and velocity correlations.

IV. SUMMARY AND CONCLUSION

We studied the effect of Coulomb friction on the granular temperature ratio, orientational correlation (coupling between translational and rotational velocities), velocity distribution functions (VDF), and density and spatial velocity correlations in the uniform shear flow of a dilute granular gas. Event-driven simulations with Lees-Edwards boundary conditions have been employed using a three-parameter collision model [30,31] that incorporates both normal (e) and tangential (β) restitution coefficients as well as Coulomb friction (μ). It has been argued that this is the minimal collision model for frictional particles since it incorporates both sliding and sticking type contacts. It is known that the translational (T) and rotational (θ) granular temperatures are unequally partitioned in a rough granular gas, except in the singular case of perfectly rough particles ($\beta = 1$); our results suggest that the degree of nonequipartition between two granular temperatures is enhanced with the inclusion of friction.

We found that the friction has a *dual role* of enhancing and diminishing the orientational correlation, depending on the particle roughness (β_0) and the friction coefficient (μ). The increase/decrease of orientational correlation occurs near the perfectly rough ($\beta \sim 1$) and smooth ($\beta \sim -1$) limits, respectively, for a range of μ from the sticking limit of $\mu \to \infty$. Below some threshold value of $\mu = \mu^c \sim 0.2$, the orientational correlation again decreases (for any β_0), eventually approaching the value for the degenerate case of smooth particles ($\beta = -1$) in the limit of zero friction ($\mu \to 0$). We speculate that the observed *nonmonotonic* dependence of orientational correlation on μ (for given β_0 and e) is due to how energy is transferred between translational and rotational modes—this needs to be investigated in future.

In a driven system the VDFs are always non-Gaussian as we confirmed in the present shear flow of a frictional granular gas. The functional form of the deviations of VDFs from a Gaussian [Eq. (18)] takes the well-known form of a double-well potential in the low-velocity regions as found in previous studies of a smooth granular gas. However, the high-velocity tails of both translational and rotational VDFs can deviate strongly from a Gaussian (depending on the values of two restitution coefficients and Coulomb friction), and have been characterized in terms of stretched exponentials [$P(C) \sim \exp(-\delta C^\alpha)$, with $\alpha < 2$]. We found that the tails of both VDFs undergo a transition from stretched exponential to Gaussian with decreasing friction coefficient (μ) in the elastic limit ($e = 1$) at any roughness β_0. The degree of

non-Gaussianity (which is measured in terms of the kurtosis κ of respective VDFs as well as in terms of the exponent of the stretched exponential high-velocity tails, α) decreases with decreasing μ for dissipative collisions ($e < 1$). We found that the Coulomb friction is responsible for enhanced density and velocity correlations for a given normal restitution coefficient e. These correlations, together with orientational correlation, seem to be responsible for non-Gaussian tails around the sticking limit.

The latter finding of a Gaussian distribution in the double limit of $\mu \to 0$ and $e \to 1$ (at any critical roughness) can be understood from the Boltzmann equation. The Boltzmann equation for the single particle distribution function, $f_1 \equiv f(\mathbf{v}_1, \boldsymbol{\omega}_1, \mathbf{r}, t)$, is

$$\frac{\partial f_1}{\partial t} + \mathbf{v}_1 \cdot \boldsymbol{\nabla} f_1 = \mathcal{C}(f, f'; e, \beta_0, \mu), \tag{24}$$

where the collision integral is given by [36]

$$\mathcal{C}(\cdot) = \frac{d^2}{2} \int_{\mathbf{k}\cdot\mathbf{g}_{12}>0} [(eJ)^{-1} f_1 f_2 - f_1' f_2'](\mathbf{k}\cdot\mathbf{g}_{12}) d\mathbf{k} d\mathbf{v}_2 d\boldsymbol{\omega}_2, \tag{25}$$

with the prime on a distribution function representing its postcollisional value; $J(e, \beta_0, \Phi)$ is the determinant of the Jacobian of transformation from precollisional to postcollisional particle velocities:

$$J(e, \beta_0, \Phi) = \left| \frac{\partial(\mathbf{v}_1', \mathbf{v}_2', \boldsymbol{\omega}_1', \boldsymbol{\omega}_2')}{\partial(\mathbf{v}_1, \mathbf{v}_2, \boldsymbol{\omega}_1, \boldsymbol{\omega}_2)} \right| = \begin{cases} e\beta_0^2, & \Phi \leqslant \Phi_0, \\ e\beta(\Phi)^2, & \Phi > \Phi_0, \end{cases} \tag{26}$$

where Φ_0 is the critical impact angle, Eq. (11). Considering the *sliding limit* of small friction (i.e., $\mu \to 0$, or, $\cot \Phi_0 \to 0$), we find from Eq. (12) that the tangential restitution coefficient,

$$\beta(\Phi) \to -1 \quad \forall \quad \beta_0, \tag{27}$$

approaches a value that coincides with the limiting case of perfectly smooth particles. In this case, the Jacobian of transformation is $J(e, \beta_0, \Phi) = e\beta(\Phi)^2 \to e$, irrespective of critical roughness β_0. Clearly, $J \to 1$ in the double limit of $e \to 1$ and $\mu \to 0$, for which case the solution of the Boltzmann equation is well known, i.e., a Maxwellian (Gaussian). This agrees with the findings of our simulations.

The above discussion suggests that the Chapman-Enskog-type perturbative expansion around the smooth limit of a frictional granular gas (with Maxwellian being the zeroth-order solution) will hold at any value of critical roughness β_0. More importantly, given the prevalence of orientational correlation at any roughness and its nonmontonic variation with Coulomb friction, it must be incorporated in the theory of frictional granular gases even in the Boltzmann limit. Last, the high-velocity tails of VDFs in a shear flow with Coulomb friction should be theoretically analyzed so that a comparison with present findings of stretched exponential tails can be made.

ACKNOWLEDGMENTS

M.A. acknowledges financial support from the DAE-SRC award (Grant No. DAE/MA/4265) by the Department of Atomic Energy, Government of India.

[1] H. M. Jaeger, S. R. Nagel, and R. P. Behringer, Rev. Mod. Phys. **68**, 1259 (1996); L. P. Kadanoff, *ibid.* **71**, 435 (1999); J. M. Ottino and D. V. Khakhar, *ibid.* **32**, 55 (2000); I. Goldhirsch, Rev. Mod. Phys. **35**, 267 (2003); I. S. Aranson and L. S. Tsimring, Rev. Mod. Phys. **78**, 1641 (2006).

[2] N. V. Brilliantov and T. Pöschel, *Kinetic Theory of Granular Gases* (Oxford University Press, Oxford, UK, 2004); P. K. Haff, J. Fluid Mech. **134**, 401 (1983); J. T. Jenkins and M. W. Richman, *ibid.* **171**, 53 (1985); J. J. Brey, J. W. Dufty, and A. Santos, J. Stat. Phys. **97**, 281 (1999); V. Kumaran, J. Fluid Mech. **561**, 1 (2006).

[3] C. K. K. Lun, J. Fluid Mech. **233**, 539 (1991).

[4] N. Sela and I. Goldhirsch, J. Fluid Mech. **361**, 41 (1998).

[5] A. Goldshtein and M. Shapiro, J. Fluid Mech. **282**, 75 (1995).

[6] N. V. Brilliantov and T. Pöschel, Europhys. Lett. **74**, 424 (2006); S. H. Noskowicz, O. Bar-Lev, D. Serero, and I. Goldhirsch, *ibid.* **79**, 60001 (2007); A. Santos, Phys. Rev. Lett. **100**, 078003 (2008).

[7] S. Esipov and T. Pöschel, J. Stat. Phys. **86**, 1385 (1997).

[8] T. van Noije and M. Ernst, Gran. Matt. **1**, 52 (1998).

[9] Y. Taguchi and H. Takayasu, Europhys. Lett. **30**, 499 (1995).

[10] A. Puglisi, V. Loreto, U. M. Marconi, A. Petri, and A. Vulpiani, Phys. Rev. Lett. **81**, 3848 (1998).

[11] J. J. Brey, D. Cubero, and M. J. Ruiz-Montero, Phys. Rev. E **59**, 1256 (1999).

[12] R. Cafiero, S. Luding, and H. J. Herrmann, Phys. Rev. Lett. **84**, 6014 (2000).

[13] J. M. Montanero and A. Santos, Gran. Matt. **2**, 53 (2000).

[14] S. J. Moon, M. D. Shattuck, and J. B. Swift, Phys. Rev. E **64**, 031303 (2001).

[15] A. Kawarada and H. Hayakawa, J. Phys. Soc. Jpn. **73**, 2037 (2004).

[16] J. S. van Zon and F. C. MacKintosh, Phys. Rev. Lett. **93**, 038001 (2004).

[17] M. Alam and V. K. Chikkadi, J. Fluid Mech. **653**, 175 (2010); K. C. Vijayakumar and M. Alam, Phys. Rev. E **75**, 051306 (2007).

[18] W. Losert, D. Cooper, J. Delour, A. Kudroli, and J. P. Gollub, Chaos **9**, 682 (1999).

[19] F. Rouyer and N. Menon, Phys. Rev. Lett. **85**, 3676 (2000).

[20] I. S. Aranson and J. S. Olafsen, Phys. Rev. E **66**, 061302 (2002).

[21] P. M. Reis, R. A. Ingale, and M. D. Shattuck, Phys. Rev. E **75**, 051311 (2007).

[22] M. Schmick and M. Markus, Phys. Rev. E **78**, 010302 (2008).

[23] H.-Q. Wang, K. Feitosa, and N. Menon, Phys. Rev. E **80**, 060304(R) (2009).

[24] S. Tatsumi, Y. Murayama, H. Hayakawa, and M. Sano, J. Fluid Mech. **641**, 521 (2009).

[25] Y. Forterre and O. Pouliquen, Annu. Rev. Fluid Mech. **40**, 1 (2008).

[26] S. B. Savage, Adv. Appl. Mech. **24**, 289 (1984).
[27] P. C. Johnson and R. Jackson, J. Fluid Mech. **176**, 67 (1987).
[28] M. Alam and P. R. Nott, J. Fluid Mech. **343**, 267 (1997).
[29] A. J. Liu and S. R. Nagel, Annu. Rev. Condens. Matter Phys. **1**, 347 (2010).
[30] O. R. Walton and R. Braun, J. Rheol. **30**, 949 (1986).
[31] O. R. Walton, In *Particulate Two-Phase Flow*, edited by M. C. Roco (Butterworth-Heinemann, New York, USA, 1993).
[32] C. K. K. Lun, Phys. Fluid **6**, 2253 (1994); C. K. K. Lun and A. A. Bent, J. Fluid Mech. **258**, 335 (1994).
[33] J. T. Jenkins and C. Zhang, Phys. Fluid **14**, 1228 (2002).
[34] M. Huthmann and A. Zippelius, Phys. Rev. E **56**, R6275 (1997).
[35] O. Herbst, R. Cafiero, A. Zippelius, H. J. Herrmann, and S. Luding, J. Phys. Chem. B **17**, 107102 (2005).
[36] I. Goldhirsch, S. H. Noskowicz, and O. Bar-Lev, Phys. Rev. Lett. **95**, 068002 (2005); J. Phys. Chem. **109**, 21449 (2005); J. Phys.: Condens. Matter **17**, S2591 (2005).
[37] R. Cafiero, S. Luding, and H. J. Herrmann, Europhys. Lett. **60**, 854 (2002).
[38] B. Gayen and M. Alam, Phys. Rev. Lett. **100**, 068002 (2008).
[39] N. V. Brilliantov, T. Pöschel, W. T. Kranz, and A. Zippelius, Phys. Rev. Lett. **98**, 128001 (2007); W. T. Kranz, N. V. Brilliantov, T. Pöschel, and A. Zippelius, Eur. J. Phys. ST **179**, 91 (2009).
[40] G. H. Bryan, in *Report of the 64th Annual Meeting of the British Association for the Advancement of Science*, edited by John Murray (London, UK, 1894), pp. 64–105.
[41] F. B. Pidduck, Proc. R. Soc. London, Ser. A **101**, 101 (1922).
[42] S. Chapman and T. G. Cowling, *The Mathematical Theory of Non-uniform Gases* (Cambridge University Press, Cambridge, UK, 1970).
[43] N. Mitarai, H. Hayakawa, and H. Nakanishi, Phys. Rev. Lett. **88**, 174301 (2002).
[44] B. Gayen and M. Alam, J. Fluid Mech. **367**, 195 (2006).
[45] S. F. Foerster, M. Y. Louge, H. Chang, and K. Allia, Phys. Fluids **6**, 1108 (1994).
[46] S. Luding, Phys. Rev. E **52**, 4442 (1995).
[47] T. Pöschel and T. Schwager, *Computational Granular Dynamics* (Springer-Verlag, Berlin, 2005).
[48] K. L. Johnson, *Contact Mechanics* (Cambridge University Press, Cambridge, UK, 1985).
[49] N. Maw, J. R. Barbar, and J. N. Fawcett, Wear **38**, 101 (1976).
[50] N. Maw, J. R. Barbar, and J. N. Fawcett, Trans. ASME: J. Lubr. Tech. **103**, 74 (1981).
[51] M. P. Allen and D. J. Tildesley, *Computer Simulation of Liquids* (Oxford University Press, Oxford, UK, 1987).
[52] A. Lees and S. F. Edwards, J. Phys. C **5**, 1921 (1972).
[53] B. Lubachevsky, J. Comput. Phys. **94**, 255 (1991).
[54] M. A. Hopkins and M. Y. Louge, Phys. Fluids **3**, 47 (1991); I. Goldhirsch and G. Zanetti, Phys. Rev. Lett. **70**, 1619 (1993); M. L. Tan and I. Goldhirsch, Phys. Fluids **9**, 856 (1996); S. Luding and H. J. Herrmann, Chaos **9**, 673 (1999); S. L. Conway and B. J. Glasser, Phys. Fluids **16**, 509 (2004); M. Alam and S. Luding, *ibid.* **17**, 063303 (2005); V. Chikkadi and M. Alam, Phys. Rev. E **80**, 021303 (2009); M. Alam, V. Chikkadi, and V. Gupta, Eur. J. Phys. ST **179**, 69 (2009).
[55] J. T. Jenkins and M. W. Richman, J. Fluid Mech. **192**, 313 (1988).
[56] I. Goldhirsch and M.-L. Tan, Phys. Fluids **8**, 1752 (1996); N. Sela, I. Goldhirsch, and S.-N. Noskowicz, *ibid.* **8**, 2337 (1996).
[57] J. J. Brey, M. J. Ruiz-Montero, and F. Moreno, Phys. Rev. E **55**, 2846 (1997).
[58] O. Pouliquen, Phys. Rev. Lett. **93**, 248001 (2004).
[59] O. Baran, D. Ertas, T. C. Halsey, G. S. Grest, and J. B. Lechman, Phys. Rev. E **74**, 051302 (2006).